THE DYNAMICAL DISTINCTION BETWEEN ELLIPTICAL AND LENTICULAR GALAXIES IN DISTANT CLUSTERS: FURTHER EVIDENCE FOR THE RECENT ORIGIN OF S0 GALAXIES

Sean M. Moran,[1] Boon Liang Loh,[2] Richard S. Ellis,[1] Tommaso Treu,[3]
Kevin Bundy,[4] and Lauren A. MacArthur[1]

ABSTRACT

We examine resolved spectroscopic data obtained with the Keck II telescope for 44 spheroidal galaxies in the fields of two rich clusters, Cl 0024+16 ($z = 0.40$) and MS 0451−03 ($z = 0.54$) and contrast this with similar data for 23 galaxies within the redshift interval $0.3 < z < 0.65$ in the GOODS northern field. For each galaxy we examine the case for systemic rotation, derive central stellar velocity dispersions σ and photometric ellipticities ϵ. Using morphological classifications obtained via *Hubble Space Telescope* imaging as the basis, we explore the utility of our kinematic quantities in distinguishing between pressure-supported ellipticals and rotationally supported lenticulars (S0s). We demonstrate the reliability of using the $v/(1 - \epsilon)$ versus σ and v/σ versus ϵ distributions as discriminators, finding that the two criteria correctly identify $63\% \pm 3\%$ and $80\% \pm 2\%$ of S0s at $z \sim 0.5$, respectively, along with $76^{+8}_{-3}\%$ and $79\% \pm 2\%$ of ellipticals. We test these diagnostics using equivalent local data in the Coma Cluster, and find that the diagnostics are similarly accurate at $z = 0$. Our measured accuracies are comparable to the accuracy of visual classification of morphologies, but avoid the band-shifting and surface brightness effects that hinder visual classification at high redshifts. As an example application of our kinematic discriminators, we then examine the morphology-density relation for elliptical and S0 galaxies separately at $z \sim 0.5$. We confirm, from kinematic data alone, the recent growth of rotationally supported spheroidals. We discuss the feasibility of extending the method to a more comprehensive study of cluster and field galaxies to $z \simeq 1$, in order to verify in detail the recent density-dependent growth of S0 galaxies.

Subject headings: galaxies: clusters: general — galaxies: elliptical and lenticular, cD — galaxies: evolution — galaxies: spiral — galaxies: stellar content

Online material: color figures

1. INTRODUCTION

Understanding the origin of the Hubble sequence remains a fundamental goal in extragalactic astronomy. The lasting utility of Hubble's classification scheme lies in its ability to distinguish between both the *dynamics* and *stellar populations* of disk and spheroidal galaxies. However, despite considerable progress in unraveling the time evolution of elliptical and spiral galaxies (see Ellis 2007 for a recent review), there is still some disagreement concerning the origin of lenticular (or S0) galaxies, a hybrid class with kinematic characteristics of disk galaxies, but whose present-day stellar populations resemble those seen in ellipticals (Es). Were S0s created ab initio or do they represent spirals whose gas supply was more recently exhausted? Understanding the origin of this intriguing population is important in resolving the extent to which galaxies are morphologically influenced by their environment.

The idea that infalling cluster spirals have somehow been converted into S0s has received much support because of the presence of a local *morphology-density relation* (Dressler 1980) and evidence of its evolution (Dressler et al. 1997; Treu et al. 2003).

However, detailed studies of local S0s have failed to resolve the question of whether they are faded remnants of early spirals (cf. Poggianti et al. 2001 vs. Burstein et al. 2005), or if they instead have similar formation histories to ellipticals, but with different bulge-to-disk ratios. The most direct approach to resolving this debate would be to directly track the evolution in the S0 and elliptical fractions with lookback time, thus tracing the formation histories of the two classes independently.

Considerable progress has been made in tracking the evolving fraction of spheroidals, f_{E+S0}, as a function of environmental density Σ (Smith et al. 2005; Postman et al. 2005; Capak et al. 2007). Although the morphology-density relation was apparently in place at $z \simeq 1$, it has evolved quite substantially at later times, mostly in regions of high projected density. One suggestion is that only ellipticals were present in abundance at $z \simeq 1$ ($f_{S0} < 0.1$), with subsequent growth in f_{E+S0} arising primarily via a density-dependent transformation of spirals into S0s (cf. Smith et al. 2005). This simple hypothesis could be tested by separating S0s from ellipticals, so that their fraction, f_{S0}, could be determined independently of that of ellipticals as a function of both Σ and z. If spiral transformations occurred, there should be fewer S0s in all overdense environments at $z \simeq 1$.

Morphologically distinguishing distant S0s from their elliptical counterparts via *Hubble Space Telescope* (*HST*) imaging has proved difficult because of surface brightness dimming, loss of resolution, band-shifting, and inclination effects, each of which might be redshift dependent thereby introducing biases. Postman et al. (2005) attempted to measure the S0 fraction morphologically at $z \simeq 1$, but the scatter in their S0 classifications, as determined in various ways, implies uncertainties of $\delta f_{S0} > 0.15$.

[1] Department of Astronomy, California Institute of Technology, MS 105-24, Pasadena, CA 91125; smm@astro.caltech.edu, rse@astro.caltech.edu, lam@astro.caltech.edu.
[2] Department of Physics, National University of Singapore, Singapore 119077; u0301419@nus.edu.sg.
[3] Department of Physics, University of California, Santa Barbara, CA 93106; tt@physics.ucsb.edu.
[4] Department of Astronomy, University of Toronto, Toronto, ON M5S 3H4, Canada; bundy@astro.utoronto.ca.

Although they find f_{S0} drops with redshift, the residual fraction at $z \simeq 1$ could be 0%–30%, consistent with a range of hypotheses. Recently, Desai et al. (2007) have found similarly low S0 fractions for clusters across the range $0.5 < z < 0.8$, but uncertainties and cluster to cluster variation remain equivalent to that of Postman et al. (2005).

The purpose of this paper is to explore the use of kinematic data to improve the separation of distant Es and S0s. Luminous ellipticals are pressure supported, whereas S0s have circularly rotating disks. The necessary ingredients to enable this distinction are the rotational velocity v, the central stellar velocity dispersion σ, and the photometric ellipticity ϵ. The combination of these three quantities has been famously used locally to demonstrate that, for a given ϵ, ellipticals have v/σ ratios less than that for a rotationally supported spheroid (Binney 1982). Tying morphological classifications to physical quantities (pressure, mass, and angular momentum) across all epochs should reduce redshift-dependent biases and facilitate comparison to numerical models that incorporate environmental effects (e.g., De Lucia et al. 2006).

As a result of a campaign in two intermediate-redshift ($z \simeq 0.5$) clusters, we have secured Keck spectroscopic data for a large sample of galaxies spanning a wide range of environments. Morphological classifications are available as a training set in these samples. We utilize these data to test the conjecture that a kinematic classifier can be reliably used to isolate S0s from ellipticals at $z \simeq 0.5$. After verifying that the classifiers robustly isolate S0s from ellipticals in a local cluster sample, we then use them to determine the S0 fraction as a function of environmental density, Σ, at this epoch. We show this is a promising approach and discuss the prospects for extending it to higher redshift samples so that the S0 fraction might be completely mapped as a function of Σ since $z \simeq 1$. Throughout this paper we adopt a standard cosmology with $H_0 = 70.0 \ \mathrm{km \ s^{-1} \ Mpc^{-1}}$, $\Omega_m = 0.3$, and $\Omega_\Lambda = 0.7$.

2. OBSERVATIONS

The primary data set for this paper is a comprehensive Keck spectroscopic and *HST* imaging (F814W) survey of morphologically selected spheroidals in two clusters, Cl 0024+16 ($z = 0.40$) and MS 0451−03 ($z = 0.54$; Treu et al. 2003; Moran et al. 2005). We contrast this with equivalent data taken in the northern GOODS field (Treu et al. 2005a, 2005b). The above cited articles give full details of the morphological selection and spectroscopic campaigns. Here we give a brief synopsis of the salient points.

The cluster data comprises 44 member spheroidals spanning a wide range of cluster-centric radius to rest frame $M_V = -19.9$, corresponding approximately to the luminosity limit adopted by Dressler et al. (1997) for the local and $z \sim 0.5$ morphology-density relations. To derive rest-frame absolute magnitudes (M_V), we apply k-corrections to the observed F814W photometry as in Moran et al. (2007a).

Morphological classification is discussed by Treu et al. (2003) for Cl 0024+16 and in S. M. Moran et al. (2007b, in preparation) for MS 0451−03, and has been deemed reliable to at least $M_V = -19.5$. In cases where the distinction between Es and S0s was ambiguous, we assigned the class E/S0. To the adopted magnitude limit, successful morphological distinction between Es and S0s was possible in 95% of cases, with only 5% classed E/S0. The original $z' < 22.5$ GOODS-N sample was classified in the same visual manner by one of us (R. S. E.), albeit from deeper *HST* data (Bundy et al. 2005; Treu et al. 2005a, 2005b). For this study, the sample has been restricted to the redshift range $0.3 < z < 0.65$

and cut at $M_V > -19.9$ to provide a comparison sample of 23 field spheroidals.

All spectroscopic data were taken with the DEIMOS spectrograph (Faber et al. 2003) on Keck II. The cluster sample was observed with a 900 line grating (Cl 0024) or a 600 line grating (MS 0451) in the 4500–8000 Å region, offering a resolution of $\sigma \simeq 30$–50 km s^{-1}. Typical exposure times were 2.5 hr in Cl 0024 and 4 hr in MS 0451. The field survey was designed to sample higher redshift spheroidals in the OH forest, and a 1200 line grating was used in the 6700–9300 Å region, providing a resolution of $\sigma \simeq 20$–30 km s^{-1}; exposure times for the brighter objects considered here were typically 4 hr. In planning the spectroscopic observations, it was not always possible to align the slit along the major axis. We discarded galaxies where the orientational mismatch was greater than $45°$, and for those with a smaller misalignment we apply a correction to the measured velocities in our analysis below (§ 3).

3. KINEMATIC MEASUREMENTS

All spectra were reduced using the DEEP2 pipeline (Davis et al. 2003) using procedures described by Moran et al. (2005) and Treu et al. (2005b). Central stellar velocity dispersions for both field and cluster spheroidals come from these analyses. Comprehensive tests were undertaken to evaluate both instrumental and algorithmic uncertainties, with the results indicating that the dispersions are accurate to <10%.

Resolved (rotational) velocity data were secured via an extension of the cross-correlation technique used to determine velocity dispersions. Our resolved 2D spectra consist of a number of individual spectra, one for each pixel across the spatial dimension of the slit. To ensure reliable measurements, every 2D spectrum was rebinned along the spatial dimension to secure a minimum average signal-to-noise ratio (S/N) of 3 (Å^{-1}) per bin. Galaxies with less than three spatial bins of sufficient S/N were removed; for our typical seeing of $0.7''$, this defines the minimum extent where a velocity gradient can be resolved.

For each of these spatial bins (with one spectrum for each), we independently determine the best-fitting velocity relative to the galaxy's mean redshift, via a cross-correlation with spectra of eight template G/K stars, shifted to the redshift of the galaxy. The resulting rotation curves were averaged across all eight template fits. We then perform a linear least-squares fit to the data points, and define the rotational velocity, v, as half the velocity range of the fitted line from end to end of the measured curve. A simple fit is justified, because unlike emission-line data, our absorption line curves rarely extend far enough to reach the characteristic "turnover," v_{rot}, of a disk rotation curve. The uncertainty in v was taken to be the larger of the rms deviation of each data point from the fitted line and the rms deviation of each velocity measurement across template fits.

The allowed misalignment between the galaxy major axis and the spectroscopic slit can reduce the measured v by up to ~40%. We make a first-order correction to the measured velocities by dividing by a factor of cos δ, where δ is the angle between the galaxy major axis and the long axis of the spectroscopic slit. Such a correction is generally only valid under the assumption that each galaxy is a thin disk (Kapferer et al. 2006), yet our sample contains both disk and spheroidal galaxies. In practice, however, the magnitude of the correction is negligible for slowly rotating or nonrotating spheroidals, and so only truly rotating disks will have their measured velocities altered significantly.

Figure 1 displays a sample of images alongside the respective rotation curves. To measure photometric parameters of each galaxy, we make use of the GALFIT software (Peng et al. 2002),
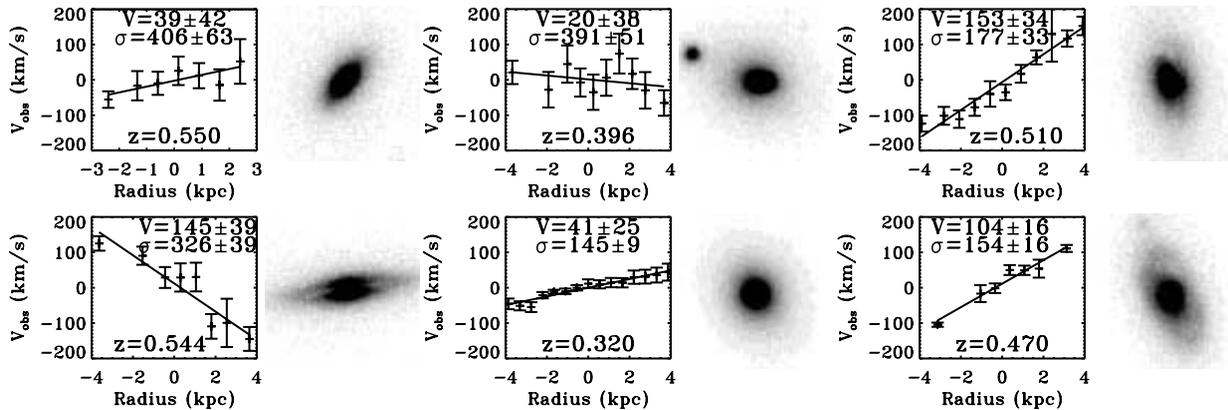
Fig. 1.— Selection of *HST* F814W images and rotation curves for both field and cluster spheroidals. *From top left to bottom right*: Two cluster ellipticals, two cluster S0s, one field E, and one field S0. In each case the redshift z, rotational velocity v, and stellar velocity dispersion σ, are listed with their errors.

fitting each galaxy to a 2D model following the Sérsic profile (see, e.g., Moran et al. 2005). In each model, the Sérsic parameter n, position angle (PA), ellipticity (ϵ), and effective radius (R_e) are allowed to vary freely, and each model is convolved with a point-spread function (PSF) derived from a star observed in the same *HST* mosaic. For the analysis discussed below, we adopt the fitted values of ϵ and R_e. Typically our measured absorption line rotation curves extend to about $0.25R_e$. Measured rotation velocities, velocity dispersions, ellipticities, and other basic information for all 67 galaxies in our combined cluster and field sample are listed in Table 1.

4. KINEMATIC CLASSIFIERS

In identifying pressure-supported ellipticals from kinematic parameters, we began by considering the $v/\sigma-\epsilon$ distribution originally proposed by Binney (1982), where $v/\sigma^* \approx v/\sigma[(1-\epsilon)/\epsilon]^{1/2} > 1$ indicates a rotationally supported spheroid. Unfortunately, our rotation curves do not extend to large enough radius to reliably measure the maximum rotation, $v_{\rm rot}$. Also, in the case of S0s, the central velocity dispersion arises partly from the prominent spheroidal component, rather than the disk. This mixing of bulge and disk information illuminates a more fundamental problem: since the (Binney 1982) criterion is meant to measure the degree of rotational support for a single spheroid, it is not a sensible test to apply to a two-component bulge-plus-disk S0. Consequently, we deemed the v/σ^* ratio to be ineffective for our purposes.

Instead, we approached the problem by minimizing a figure of merit $\Delta = \Sigma_i(T_{{\rm dyn},i} - T_{{\rm morph},i})^2$ for various classifiers. Here $T_{\rm dyn}$ is a proposed kinematic classifier based on some combination of the three key variables, v, σ, and ϵ, and $T_{\rm morph}$ is the *HST*-based type, E ($T = 0$), E/S0 ($T = 1$), or S0 ($T = 2$). In order to use the visual morphologies to calibrate our kinematic classifiers in this way, we must ensure that our visual classification is unbiased. In some local samples, a deficit of face-on S0s seems to indicate that many are misidentified as ellipticals (Jørgensen & Franx 1994). In Figure 2, we display cumulative histograms of ellipticity for Es and S0s in our combined cluster and field sample of 67 sources (*in red*). It is clear from the figure that the distributions of ellipticities in our sample are consistent with the gray model curves overplotted, which indicate a Gaussian distribution of ellipticities with randomly distributed inclinations. As such, our sample is an appropriately unbiased calibrator for our kinematic classifiers. After minimizing Δ for several candidate indicators, we found that the combinations $v/(1 - \epsilon)$ versus σ and v/σ versus ϵ were the most successful, both yielding a higher success rate than the canonical v/σ^*.

The former criterion yields optimal separation of Es and S0s when we classify galaxies with $v/(1 - \epsilon) > 85 \pm 5 \,{\rm km\,s^{-1}}$ as S0s. We note that this choice of kinematic classifier does not strictly require a measurement of σ, and so can be applied to observations where σ is unavailable. Overall, the criterion recovers $63\% \pm 3\%$ of the 35 S0s and $76^{+8}_{-3}\%$ of the 29 Es in our sample (Fig. 3, *bottom*). Given there is inevitably some morphological misclassification at the 10%–20% level (Ellis et al. 1997; Treu et al. 2003), this seems an adequate success rate. Specifically, all but two of the morphological S0s below the 85 km s^{-1} limit display no rotation, i.e., they are consistent with $v < 30$ km s^{-1}, and those morphological Es above the limit are mostly rotating with $v \simeq 60$–180 km s^{-1}. Of course, the most critical test of this discriminator is not its success rate at identifying individual galaxies, but rather how well it estimates the overall fraction of S0s. Morphologically, our sample contains $43\% \pm 8\%$ ellipticals and $52\% \pm 8\%$ S0s, with the remaining 5% ambiguous E/S0s; note that we do not yet include any accounting for spiral galaxies. The $v/(1 - \epsilon)$ discriminator yields an S0 fraction of $43\% \pm 5\%$, which is consistent within the errors of the visually classified proportion.

We then considered a criterion that exploits σ as well. While the previous criterion was practical and effective, it was solely concerned with detection of rotation for a given shape. The addition of σ introduces a measure of pressure support, and thus should be a more robust indicator of the presence of a bulge. Specifically, if we define ellipticals to have $v/\sigma < 0.50 \pm 0.03$ and $\epsilon < 0.3$, a somewhat higher degree of success is revealed: we correctly identify $80\% \pm 2\%$ and $79\% \pm 2\%$ of S0s and ellipticals, respectively (Fig. 3, *top*). Likewise, the predicted overall fraction of S0s, $51\% \pm 3\%$, is in excellent agreement with its morphological equivalent.

Naturally, once we calibrate our kinematic classifiers against our $z \sim 0.5$ sample, it is essential that we validate its performance against an independent set of data. As our goal is to develop a morphological discriminator that is more redshift invariant than visual classification, it makes sense to choose a comparison sample at a much different redshift. Accordingly, we independently applied both kinematic classifiers to a local sample of 35 Es and S0s in the Coma Cluster (Mehlert et al. 2000), supplemented by an additional 11 mostly elliptical galaxies from Bender & Nieto (1990). The distribution of ellipticities of S0s in this sample does appear to suffer from the bias identified by Jørgensen & Franx (1994; Fig. 2). However, since we are not directly calibrating our kinematic indicators on this local comparison sample, the bias in the sample will not prevent us from evaluating the performance of our indicators at low redshift. With our small sample size, we

TABLE 1

MEASUREMENTS OF CL 0024+16, MS 0451−03, AND FIELD GALAXIES

ID	R.A. (deg)	Decl. (deg)	z	v (km s^{-1})	σ (km s^{-1})	ϵ	Visual Morphology	δ (deg)
C1	6.682304	17.138241	0.397	137 ± 9	211 ± 11	0.24	S0	15
C2	6.726579	17.140829	0.393	65 ± 9	234 ± 22	0.25	E	12
C3	6.536877	17.165190	0.397	86 ± 20	186 ± 24	0.39	S0	12
C4	6.649991	17.162821	0.391	<60	262 ± 25	0.05	E	26
C5	6.643103	17.172791	0.386	48 ± 23	215 ± 22	0.19	E	42
C6	6.782351	17.180410	0.397	101 ± 10	209 ± 16	0.16	S0	5
C7	6.631488	17.286880	0.393	141 ± 10	182 ± 20	0.78	S0	38
C8	6.514315	17.317190	0.395	<29	227 ± 29	0.21	E	9
C9	6.631382	17.101040	0.398	41 ± 18	128 ± 42	0.17	E/S0	2
C10	6.640234	17.158600	0.392	53 ± 15	195 ± 22	0.60	S0	25
C11	6.660044	17.166290	0.398	41 ± 8	129 ± 22	0.37	E/S0	4
C12	6.645772	17.172569	0.388	62 ± 13	173 ± 18	0.10	E	39
C13	6.630862	17.174200	0.395	23 ± 8	137 ± 21	0.33	S0	44
C14	6.630893	17.182131	0.396	<58	391 ± 51	0.24	E	45
C15	6.613021	17.207199	0.398	23 ± 19	204 ± 30	0.08	E	3
C16	6.595411	17.208710	0.397	33 ± 15	150 ± 25	0.14	S0	20
C17	6.589549	17.236601	0.396	63 ± 9	150 ± 16	0.25	S0	35
C18	6.741905	17.266029	0.390	7 ± 4	87 ± 19	0.27	E/S0	20
C19	6.629107	17.285839	0.396	46 ± 8	120 ± 18	0.55	S0	12
C20	6.499555	17.336269	0.395	39 ± 11	131 ± 15	0.60	S0	36
C21	73.520592	−3.096000	0.510	153 ± 34	177 ± 33	0.40	S0	16
C22	73.520485	−3.000458	0.542	30 ± 24	320 ± 21	0.18	E	6
C23	73.523880	−3.011362	0.539	34 ± 21	243 ± 17	0.31	E	14
C24	73.552063	−3.018945	0.532	130 ± 20	275 ± 18	0.46	E	0
C25	73.566452	−3.101381	0.550	<81	406 ± 63	0.47	E	30
C26	73.439285	−3.137721	0.545	<37	420 ± 82	0.30	E	31
C27	73.442268	−2.900079	0.552	<81	254 ± 23	0.27	E	41
C28	73.530807	−3.091694	0.546	93 ± 44	313 ± 36	0.65	S0	33
C29	73.496529	−2.947528	0.548	<38	227 ± 17	0.22	E	1
C30	73.512939	−2.932262	0.544	145 ± 39	326 ± 39	0.67	S0	30
C31	73.501221	−2.982960	0.533	51 ± 30	234 ± 27	0.51	S0	25
C32	73.559761	−3.025668	0.540	<26	190 ± 26	0.23	S0	6
C33	73.545235	−3.014432	0.539	<50	366 ± 52	0.24	E	16
C34	73.540581	−3.004315	0.545	<35	188 ± 18	0.33	E	9
C35	73.545334	−3.026837	0.535	<23	136 ± 10	0.33	S0	23
C36	73.541374	−3.024953	0.539	66 ± 27	210 ± 17	0.44	S0	30
C37	73.558983	−2.991541	0.532	<41	249 ± 40	0.10	E	26
C38	73.579918	−2.990385	0.531	21 ± 20	68 ± 24	0.68	E	41
C39	73.601814	−3.064165	0.546	78 ± 27	250 ± 24	0.74	S0	29
C40	73.600838	−3.060720	0.536	42 ± 19	177 ± 14	0.01	E	21
C41	73.690582	−3.034126	0.543	151 ± 43	328 ± 25	0.38	E	33
C42	73.664803	−3.084279	0.540	57 ± 31	273 ± 15	0.67	S0	27
C43	73.555710	−3.012476	0.532	<41	233 ± 46	0.71	S0	0
C44	73.535393	−3.009354	0.526	78 ± 15	159 ± 20	0.67	S0	0
F1	189.339612	62.226372	0.48	81 ± 25	244 ± 18	0.18	E	15
F2	189.374580	62.216985	0.51	<24	191 ± 20	0.14	E	17
F3	189.488759	62.263352	0.46	<20	236 ± 20	0.15	E	40
F4	189.220348	62.245666	0.32	41 ± 25	145 ± 9	0.21	E	6
F5	189.200321	62.219268	0.47	56 ± 13	124 ± 13	0.12	E	2
F6	189.252330	62.209726	0.56	<40	118 ± 13	0.09	E	27
F7	189.013560	62.186461	0.64	24 ± 17	114 ± 25	0.14	E	39
F8	189.073642	62.229072	0.53	85 ± 31	171 ± 12	0.13	E	5
F9	189.308295	62.343580	0.53	<35	206 ± 23	0.28	E	19
F10	189.359264	62.229837	0.47	104 ± 16	154 ± 16	0.48	S0	2
F11	189.359027	62.234295	0.48	<41	313 ± 45	0.44	S0	2
F12	189.434130	62.232987	0.51	25 ± 17	73 ± 8	0.33	S0	32
F13	189.472041	62.248390	0.51	114 ± 10	138 ± 10	0.24	S0	22
F14	189.469027	62.247062	0.51	88 ± 15	164 ± 17	0.47	S0	1
F15	189.477354	62.257551	0.46	31 ± 10	121 ± 13	0.26	S0	25
F16	189.262189	62.239978	0.51	<120	147 ± 23	0.34	S0	11
F17	189.172782	62.234202	0.56	<19	167 ± 14	0.19	S0	13
F18	189.360790	62.287180	0.56	<13	166 ± 13	0.06	S0	11

TABLE 1—*Continued*

ID	R.A. (deg)	Decl. (deg)	z	v (km s^{-1})	σ (km s^{-1})	ϵ	Visual Morphology	δ (deg)
F19	189.142570	62.242571	0.52	52 ± 49	195 ± 27	0.37	S0	5
F20	189.095001	62.216703	0.47	58 ± 17	173 ± 22	0.48	S0	16
F21	189.063660	62.206127	0.32	46 ± 9	81 ± 15	0.42	S0	40
F22	189.158314	62.291520	0.56	74 ± 19	261 ± 19	0.31	S0	45
F23	189.147118	62.186147	0.41	21 ± 10	124 ± 10	0.06	S0	12

NOTES.—Galaxy IDs are designated with C for cluster members and F for field galaxies. Velocities are listed uncorrected for slit misalignment. Upper limits on velocities are 1 σ.

calculate that the bias reflected in Figure 2 implies that only 1−2 additional galaxies with incorrect visual morphologies are present in the sample, which is small compared to other sources of uncertainty.

Importantly, Mehlert et al. (2000) published full rotation curves for their galaxies, allowing us to remeasure velocities in a manner similar to that adopted in § 3. For each of their galaxies we fit a straight line to data points within radius $<0.25R_e$, thus simulating the radial extent of our curves. Such a truncated fit generally yields velocities about 40% of the velocity revealed by the full rotation curves of the local galaxies, and we expect that our $z \sim 0.5$ sample similarly underestimates rotation. Such underestimated velocities may contribute to our misidentification rate, suggesting that deeper observations at $z \geq 0.5$ may improve the accuracy of our kinematic classification.

As shown in Figure 3, the recovery is equally successful (65%−80% accuracy for individual galaxies) for both kinematic classifiers. They likewise reliably recover the correct morpho-

logical mix. The $v/(1 - \epsilon)$ discriminator predicts that the local sample consists of 30% ± 3% S0s, identical to the visually determined fraction, while the other discriminator predicts 37% ± 3%. This demonstrates no obvious redshift dependence in the classification, at least within the errors of the small available samples. In Table 2, we list the success rates achieved for each classifier on both local and $z \sim 0.5$ data, as well as the calculated S0 fractions from each method.

Locally, it has been shown that a simple cut at $\epsilon = 0.3$ effectively identifies ∼70% of S0s and an even higher fraction of Es (Jørgensen & Franx 1994), and in our $z \sim 0.5$ sample the success rate is only slightly worse (∼70% of both Es and S0s). So what, then, have we gained by adding kinematic information to this mix? The advantages are two-fold. First, while ϵ may be an accurate predictor of morphology locally, such a relation is known to break down toward higher redshift, where elongated galaxies do not necessarily reflect ordered rotation (Erb et al. 2004). Velocities and dispersions therefore become essential in separating rotating from nonrotating galaxies as we extend our current method of E−S0 discrimination to higher redshift. Being sensitive to the dynamical structure, we can also hope to be less influenced by band shifting or recent star formation, which could influence
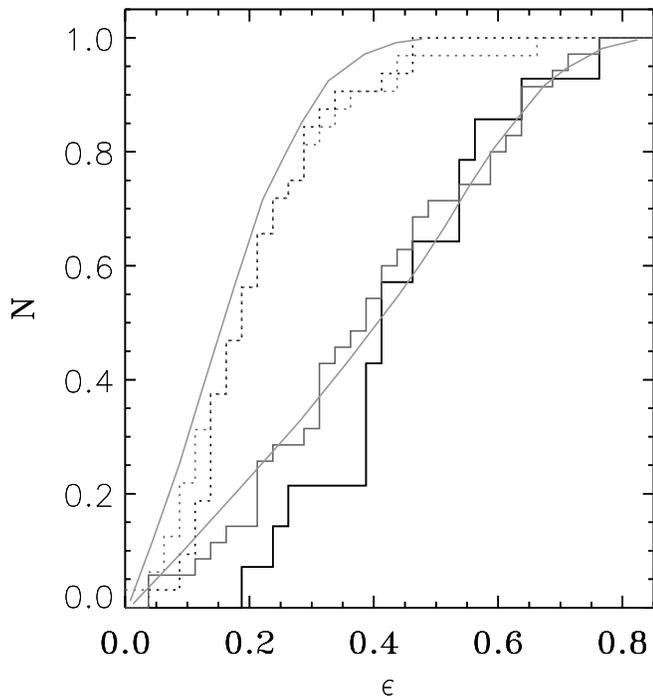

FIG. 2.—Cumulative distribution of ellipticities for galaxies in our $z \sim 0.5$ (*red*) and local (*black*) samples. Dotted histograms indicate visually classified ellipticals, and solid histograms denote S0s. The gray curves overplotted are the best-fitting Gaussian distributions of galaxy ellipticities from Jørgensen & Franx (1994). At $z \sim 0.5$, both Es and S0s are consistent with the model curves, indicating that the distributions are unbiased. The local sample exhibits the undercounting of low-ellipticity S0s discussed in Jørgensen & Franx (1994). [*See the electronic edition of the Journal for a color version of this figure.*]
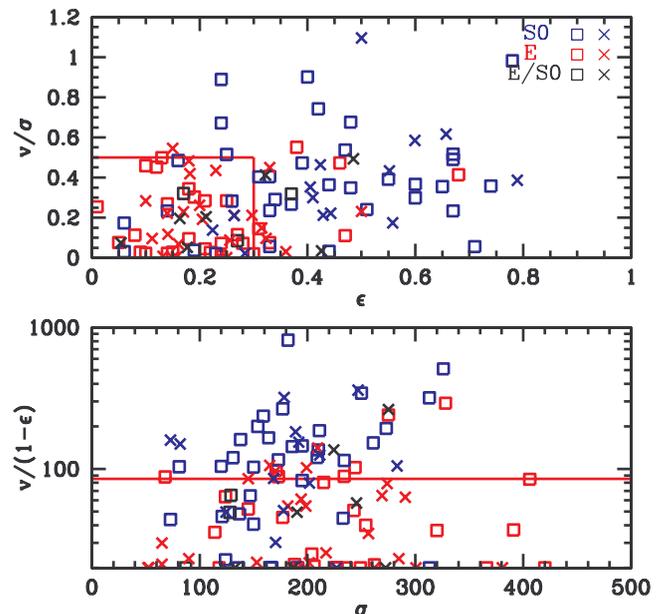

FIG. 3.—Efficacy of two kinematic classifiers in recovering morphological types in the distant cluster sample. In both cases, symbol colors denote the visually determined morphologies. Squares refer to distant cluster galaxies and crosses to those in the local sample. *Top*: v/σ vs. ϵ, adopting a limit of $v/\sigma > 0.50$ and $\epsilon > 0.3$ correctly identifies >79% of Es and S0s. *Bottom*: $v/(1 - \epsilon)$ vs. σ, adopting a rotational criterion of $v/(1 - \epsilon) > 85$ km s^{-1} is an accurate substitute, correctly identifying 63% of S0s and 76% of Es.

TABLE 2
Success Rates of Kinematic Classifiers

Sample	v/σ vs. ϵ (%)			$v/(1-\epsilon)$ vs. σ (%)			Visual f_{S0} (%)
	E	S0	f_{S0}	E	S0	f_{S0}	
$z \sim 0.5$	80 ± 2	79 ± 2	51 ± 3	63 ± 3	76^{+8}_{-2}	43 ± 5	52 ± 8
$z \sim 0.0$	79 ± 3	76 ± 3	37 ± 3	64 ± 3	80 ± 2	30 ± 3	30 ± 8

Notes.— For each kinematic discriminator we list under heading E (S0) the fraction of visually determined Es (S0s), where the kinematic discriminator yields the same class. Under f_{S0} we indicate the overall fraction of S0s predicted by applying each kinematic classifier, in comparison to the visually determined f_{S0} at right.

the measurement of ellipticity. Second, applying two different kinematic indicators, such as those presented here, adds confidence to the determination of the morphological mix, so long as the two indicators yield consistent measures of the S0 fraction. Overall, then, ellipticity is most usefully combined with measures of rotation and velocity dispersion in order to assess of the morphologies of galaxies, while minimizing redshift-dependent effects.

5. EVOLUTION OF KINEMATICALLY DEFINED S0S

To demonstrate the utility of kinematic information in studying the evolution in the abundance of S0s, we now apply the kinematic classifiers to revisit the evolving morphology-density relation, tagging each galaxy according to its local environmental density, Σ, as defined in Treu et al. (2003). In constructing the fraction of S0s, f_{S0}, at $z \sim 0.5$, we assume we have representatively sampled the available population. To improve statistics in this preliminary comparison, we combine data from both clusters and contrast this with estimates in the field, for which Σ estimates have been determined following the procedures discussed in Treu et al. (2005a). To estimate f_{S0}, we first recalculate the robust visual determination of f_{E+S0} from Treu et al. (2003) into two density bins across the cluster fields and also adopt the field value from that paper. We then calculate f_{S0} by counting the number of kinematically determined ellipticals (N_E) and S0s (N_{S0}) in each density bin and the field, such that $f_{S0} = N_{S0}/(N_E + N_{S0})f_{E+S0}$.

Figure 4 illustrates the result. We find a fairly low fraction of S0s ($f_{S0} \simeq 28 \pm 6\%$) at all cluster densities, except that our sample is not yet sufficiently large to reliably probe the core regions. The local S0 fraction at comparable densities is about $f_{S0} = 50\%$ (Dressler 1980), so the kinematic data strongly support earlier contentions (Dressler et al. 1997; Postman et al. 2005) that there is a substantial decline in the S0 fraction in clusters. Interestingly, the fraction in the field is even lower, $16\% \pm 5\%$, although clearly nonzero. Larger samples would confirm these trends.

Recently, van der Marel & van Dokkum (2006) have also considered the utility of resolved kinematic data of distant cluster galaxies. Their analysis is more concerned with establishing the fraction of rotating spheroidals rather than in separating Es and S0s. Based on a much smaller sample, they find a slightly *larger* fraction of rotating Es than observed locally. We note they use the quantity v/σ^*, which we found to be ineffective for reasons discussed earlier.

Given the efficiency of multi-object spectrographs such as DEIMOS, it is interesting to consider the prospects of our method for tracing the full evolutionary history of S0s in various density regimes over $0 < z < 1$, for example in order to verify or otherwise the scenario put forward by Smith et al. (2005) and Postman et al. (2005). Visual discrimination between early- and late-type galaxies is more reliable than E−S0 separation, even up to $z > 1.0$ (Postman et al. 2005), and so our reliance on the visually

determined f_{E+S0} poses no barrier to extending this method up to $z \sim 1$.

The key challenge to extending our method to higher redshift is the loss of spatial resolution that occurs as one observes galaxies at smaller apparent sizes, with a relatively fixed ground-based seeing limit. At $z \sim 0.5$, our typical seeing of $0.7''$ FWHM corresponds to 4.3 kpc, compared to a $6-8$ kpc typical extent of our rotation curves. At $z = 1$, the same seeing disk covers a physical diameter of 5.6 kpc, 30% larger. Considering our requirement to have at least three independent spatial bins, and assuming similar signal-to-noise spectra, a similar study at $z \sim 1$ may be limited to galaxies with spatial extent $\gtrsim 8$ kpc; only about 25% of the $z \sim 0.5$ sample meet this requirement.

In fact, the situation is not so dire, as we are most interested in detecting only whether a galaxy is rotating or not, and so blurring of the velocity gradient due to seeing is only important if the velocity is smeared toward zero. To test our ability to measure $z \sim 1$ rotation curves, we have convolved our $z \sim 0.5$ curves with a Gaussian kernel to simulate the seeing at $z = 1$. Remeasuring velocities on these blurred curves, we find that our kinematic classification scheme predicts the same morphology as the unblurred curve in 96% of the objects. We thus conclude that kinematic discrimination between Es and S0s can be a powerful tool for tracing the presumed buildup of S0 galaxies even up to $z > 1$, and will provide an additional and more fundamental discriminator at these high redshift.
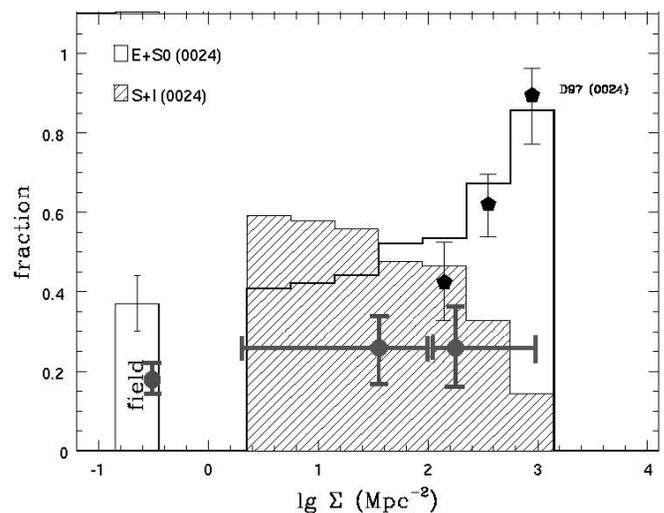

Fig. 4.— Morphology-density relation at $z \simeq 0.5$, adapted from Treu et al. (2003). Red points indicate the S0 fraction as determined from our kinematic indicators, with error bars reflecting the disagreement between discriminators, plus Poisson uncertainty. Histograms show E+S0 and Spiral+Irregular fraction from Treu et al. (2003), as indicated. Black points are E+S0 fraction from Dressler et al. (1997). [*See the electronic edition of the Journal for a color version of this figure.*]

6. CONCLUSIONS

We examine the potential of using resolved kinematics of distant galaxies to separate, independently of morphological data, elliptical and lenticular galaxies. Applying various criteria to a sample of 44 cluster galaxies and 23 field galaxies at $z \simeq 0.5$, we find promising prospects. Using the morphological classification as a starting point, we recover the morphological mix to within 10% accuracy using various combinations of the stellar rotational velocity, velocity dispersion, and ellipticity. We test the utility of our classifiers on local data and use them to establish the first kinematically based evidence for a declining fraction of S0s with redshift across a wide range of densities.

REFERENCES

Bender, R., & Nieto, J-L. 1990, A&A, 239, 97
Binney, J. 1982, ARA&A, 20, 399
Bundy, K., Ellis, R. S., & Conselice, C. 2005, ApJ, 625, 621
Burstein, D., Ho., L. C., Huchra, J. P., & Macri, L. M. 2005, ApJ, 621, 246
Capak, P., et al. 2007, ApJ, submitted (astro-ph/0703668)
Davis, M., et al. 2003, Proc. SPIE, 4834, 161
De Lucia, G., Springer, V., White, S. D. M., Croton, D., & Kauffmann, G. 2006, MNRAS, 366, 499
Desai, V., et al. 2007, ApJ, 660 1151
Dressler, A. 1980, ApJ, 236, 351
Dressler, A., et al. 1997, ApJ, 490, 577
Ellis, R. S. 2007, in Saas-Fee Advanced Course 36, First Light in the Universe (Berlin: Springer), in press
Ellis, R. S., Smail, I., Dressler, A., Couch, W. J., Oemler, A., Jr., Butcher, H., & Sharples, R. M. 1997, ApJ, 483, 582
Erb, D., Steidel, C. C., Shapley, A. E., Pettini, M., & Adelberger, K. L. 2004, ApJ, 612, 122
Faber, S. M., et al. 2003, Proc. SPIE, 4841, 1657

Jørgensen, I., & Franx, M. 1994, ApJ, 433, 553
Kapferer, W., Kronberger, T., Schindler, S., Böhm, A., & Ziegler, B. L. 2006, A&A, 446, 847
Mehlert, D., Saglia, R. P., Bender, R., & Wegner, G. 2000, A&AS, 141, 449
Moran, S. M., Ellis, R. S., Treu, T., Smail, I., Dressler, A., Coil, A. L., & Smith, G. P. 2005, ApJ, 634, 977
Moran, S. M., Miller, N., Treu, T., Ellis, R. S., & Smith, G. P. 2007a, ApJ, 659, 1138
Peng, C. Y., Ho, L., Impey, C., & Rix, H.-W. 2002, AJ, 124, 266
Poggianti, B. M., et al. 2001, ApJ, 563, 118
Postman, M., et al. 2005, ApJ, 623, 721
Smith, G. P., Treu, T., Ellis, R. S., Moran, S. M., Dressler, A. 2005, ApJ, 620, 78
Treu, T., Ellis, R. S., Kneib, J.-P., Dressler, A., Smail, I., Czoske, O., Oemler, A., & Natarajan, P. 2003, ApJ, 591, 53
Treu, T., Ellis, R. S., Liao, T. X., & van Dokkum, P. G. 2005a, ApJ, 622, L5
Treu, T., et al. 2005b, ApJ, 633, 174
van der Marel, R., & van Dokkum, P. 2006, ApJ, submitted (astro-ph/0611571)